Magnetic Nanoscaled Fe3O4/CeO2 Composite as an Efficient Fenton-Like Heterogeneous Catalyst for Degradation of 4-Chlorophenol

ARTICLE *in* ENVIRONMENTAL SCIENCE & TECHNOLOGY · AUGUST 2012

Impact Factor: 5.33 · DOI: 10.1021/es300303f · Source: PubMed

2 AUTHORS, INCLUDING:

Jianlong Wang
Tsinghua University
310 PUBLICATIONS **7,598** CITATIONS

SEE PROFILE

Environmental Science & Technology

Article

pubs.acs.org/est

Magnetic Nanoscaled Fe_3O_4/CeO_2 Composite as an Efficient Fenton-Like Heterogeneous Catalyst for Degradation of 4-Chlorophenol

Lejin Xu[†] and Jianlong Wang*[,†,‡]

[†]Laboratory of Environmental Technology, INET, and [‡]State Key Joint Laboratory of Environment Simulation and Pollution Control, Tsinghua University, Beijing 100084, People's Republic of China

Supporting Information

ABSTRACT: Magnetic nanoscaled Fe_3O_4/CeO_2 composite was prepared by the impregnation method and characterized as a heterogeneous Fenton-like catalyst for 4-chlorophenol (4-CP) degradation. The catalytic activity was evaluated in view of the effects of various processes, pH value, catalyst addition, hydrogen peroxide (H_2O_2) concentration, and temperature, and the pseudo-first-order kinetic constant of 0.11 min^{-1} was obtained for 4-CP degradation at 30 °C and pH 3.0 with 30 mM H_2O_2, 2.0 g L^{-1} Fe_3O_4/CeO_2, and 0.78 mM 4-CP. The high utilization efficiency of H_2O_2, calculated as 79.2%, showed a promising application of the catalyst in the oxidative degradation of organic pollutants. The reusability of Fe_3O_4/CeO_2 composite was also investigated after six successive runs. On the basis of the results of metal leaching, the effects of radical scavengers, intermediates determination, and X-ray photoelectron spectroscopic (XPS) analysis, the dissolution of Fe_3O_4 facilitated by CeO_2 played a significant role, and 4-CP was decomposed mainly by the attack of hydroxyl radicals (•OH), including surface-bound $•OH_{ads}$ generated by the reaction of Fe^{2+} and Ce^{3+} species with H_2O_2 on the catalyst surface, and $•OH_{free}$ in the bulk solution mainly attributed to the leaching of Fe.

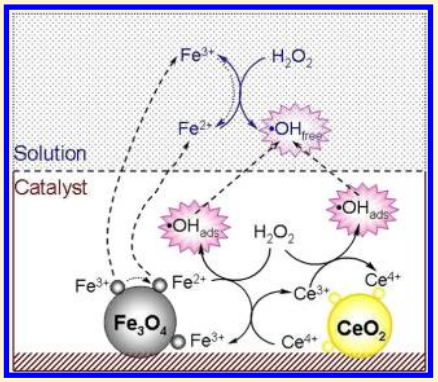

INTRODUCTION

Heterogeneous catalysts with low Fe dissolution, such as nanoparticulate zerovalent iron,[1] iron oxides,[2−4] and iron-immobilized clays,[5] are increasingly replacing homogeneous Fe^{2+}/Fe^{3+} solutions to prevent the accumulation and precipitation of soluble iron. However, many of them show weak catalytic activity, which often need the aid of ultrasound and UV/visible light irradiation, increasing the energy requirements and the cost for wastewater treatment.[6−8] Recently, ferromagnetic nanoparticles have attracted considerable attention because of their large specific surface and high surface reactivity as well as their stability and reusability.[9−11] Luo et al.[10] found that $BiFeO_3$ magnetic nanoparticles (BFO MNPs) could effectively decompose hydrogen peroxide (H_2O_2) into •OH radicals, showing excellent stability and reusability in the oxidative degradation of Rhodamine B. Yan's group[9,12] reported that Fe_3O_4 MNPs had peroxidase-like activity and could activate H_2O_2, yielding over 85% removal of phenol and about 30% mineralization within 3 h.

As is well-known, cerium, a rare earth element of the lanthanide series, has a redox cycle between the 3+ and 4+ oxidation states, providing a high oxygen storage capacity.[13−15] This property enhances the performance of transition metal catalysts used in automotive exhaust treatment and wastewater treatment.[16−18] Martins' group[19,20] investigated the catalytic activity of Fe−Ce−O particles with diameters in the range of 250−500 μm for Fenton's depuration of phenolic wastewaters. Zhang et al.[21] reported that nanoscaled Fe−Ce oxide hydrate catalyst showed a relatively low rate in heterogeneous Fenton reaction for decolorization of reactive brilliant red X-3B, which was assisted by UV irradiation to achieve almost complete removal of dye within 30 min. We anticipate that nanoscaled cerium oxide (CeO_2) can enhance the catalytic activity of Fe_3O_4 MNPs, and this novel composite is a fascinating and competitive candidate for the catalytic activation of H_2O_2. Furthermore, Heckert et al.[15] suggested that cerium might be capable of redox cycling in the presence of H_2O_2 and behaved similar to iron in a Fenton-like reaction. This interesting behavior needs to be studied in the application of ceria-based catalyst for wastewater treatment, and further work is required for the elucidation of the role of cerium and ferrum.

This paper presents our research on the catalytic properties of superparamagnetic nanoscaled Fe_3O_4/CeO_2 composite, which was used to promote the Fenton oxidation of 4-chlorophenol (4-CP) by H_2O_2. The physical and chemical characterization of Fe_3O_4/CeO_2 was conducted, and the applicability of this composite in heterogeneous Fenton reaction was evaluated in view of the effect of the main variables (e.g., pH, catalyst and H_2O_2 concentration, and temperature), reaction kinetics, the material stability, degradation mechanism, as well as the role of cerium and ferrum.

Received: March 15, 2012
Revised: June 18, 2012
Accepted: August 27, 2012
Published: August 27, 2012

dx.doi.org/10.1021/es300303f | Environ. Sci. Technol. 2012, 46, 10145−10153

MATERIALS AND METHODS

Preparation and Characterization of Catalyst. Cerium oxide nanoparticles (CeO_2 NPs) were precipitated from a solution of 100 mL of 0.1 M $Ce(NO_3)_3{\cdot}6H_2O$ with 4 g/L PEG 4000 using 150 mL of 0.1 M $(NH_4)_2CO_3$ aqueous solution. After violently stirring for 10 min at 40 °C, the formed white gel precursors were filtrated and washed with distilled water twice, and then redispersed to ethanol by ultrasonic wave (frequency 99 kHz) for 10 min. The resulting precipitate was dried at room temperature under vacuum and finally calcined at 300 °C for 1 h in air.

Fe_3O_4/CeO_2 MNPs were prepared by the impregnation method[22,23] with a known mass of CeO_2 particles and solution containing calculated amounts of $FeSO_4{\cdot}7H_2O$ and $Fe_2(SO_4)_3$. Briefly, a solution of $FeSO_4{\cdot}7H_2O$ and $Fe_2(SO_4)_3$ with a molar ratio of 1:2 was dropped into a four-necked flask containing 100 mL of 0.2 M NaOH and CeO_2 with violent stirring under Ar protecting at 80 °C, as described elsewhere.[24] After washing with water and ethanol, nanoparticles were dried at room temperature under vacuum for instant usage. The weight ratios of Fe_3O_4 and CeO_2 are 2:1, 1:1, and 1:2. Separate experimental results (Supporting Information, Figure S1) indicated that the best removal efficiency of 4-CP was obtained with the weight ratio of Fe_3O_4 and CeO_2 1:1. Therefore, the Fe_3O_4/CeO_2 composite with weight ratio of 1:1 was selected for the characterization and degradation experiments in the present work. Fe_3O_4 MNPs was synthesized as in the above procedure without adding CeO_2. All the products were stored in a desiccator under ambient temperature for further experiments. Characterization of the nanoparticles is described in the Supporting Information.

Degradation Experiment. Batch degradation experiments of 4-CP were carried out in a conical flask (25 mL) placed on a rotary shaker (TZ-2EH, Beijing Wode Co.) with the rotate speed of 150 rpm in the dark. The reaction suspension was prepared by adding the required amount of catalyst into 10 mL of a 0.78 mM 4-CP solution that had been adjusted to the desired pH value by H_2SO_4. A known concentration of H_2O_2 was added to the solution to initiate the reaction. Then, samples were taken at set intervals using a 5 mL syringe, filtered immediately through a 0.22 μm filter film, and quenched with excess *n*-butanol. To test the stability of Fe_3O_4/CeO_2 composite, the catalyst was gathered, washed, dried under vacuum, and reused in a fresh solution of 4-CP and H_2O_2 several times. Each experiment was run in triplicate, and average values and standard deviations are presented.

Sample Analysis. The concentrations of 4-CP and hydroquinone were analyzed on a high performance liquid chromatograph (Agilent 1200 Series, Agilent) equipped with a diode array detector (DAD) and a C18 reversed-phase column (5 μm, 4.6 mm ×150 mm). The mobile phase used for 4-CP was a mixture of methanol and water (60:40, v/v) at a flow rate of 1.0 mL min^{-1} with a column temperature of 30 °C, and the analytical wavelength was 280 nm. For hydroquinone analysis, the sample was analyzed at a flow rate of 0.8 mL min^{-1} with a mobile phase of methanol and water at a ratio of 50:50 (v/v) and a UV absorbance wavelength of 254 nm.

Total organic carbon values were determined by a Multi 2100 TOC/TN analyzer (Analytik Jena AG Corporation). The pH was measured with a Thermo Orion model 8103BN pH-meter. The measurements of chloride ions (Cl^-) and carboxylic acids were conducted using an ion chromatograph (Dionex model ICS 2100) coupled with a dual-piston pump, a Dionex IonPac AS19 analytical column (4 × 250 mm), an IonPac AG19 guard column (4 × 50 mm), and a DS6 conductivity detector. Suppression of the eluent was achieved with a Dionex anion ASRS 300 electrolytic suppressor (4 mm) in the autosuppression external water mode.

The concentration of ferrous ion was measured colorimetrically with 1,10-phenanthroline at 510 nm on a UV/vis spectrophotometer (Lambda 25, PerkinElmer), as described previously.[25] Total dissolved iron was analyzed also by this method using hydroxylamine hydrochloride as reducing agent.[26,27] The dissolved cerium concentration was detected by atomic absorption spectrometry (AAS6 VARIO). For H_2O_2 concentration determination, the iodimetric titration method was used.[28]

RESULTS AND DISCUSSION

Characterization of Catalysts. The characterization of pure CeO_2 NPs is provided in Figures S2–S4 of the Supporting Information (SI). The XRD pattern, HRTEM images, BET analysis, and superparamagnetic property of pure Fe_3O_4 MNPs are described in detail elsewhere.[29] Chemical and physical properties of catalysts investigated in this study are given in Table 1.

Table 1. Summary of Physicochemical Properties of CeO_2, Fe_3O_4, and Fe_3O_4/CeO_2 Nanoparticles

sample	particle size (nm)	S_{BET} (m^2 g^{-1})	pore size (nm)	pore volume (cm^3 g^{-1})	M_s (emu g^{-1})	removal of 4-CP after 60 min (%)
CeO_2	5	108.03	3.82	0.096	–	5
Fe_3O_4	10	67.79	3.85	0.039	19.6	21
Fe_3O_4/CeO_2	5–10	80.21	3.44	0.12	14.4	100

Figure 1a shows the X-ray diffractogram of Fe_3O_4/CeO_2 composite. The XRD patterns of CeO_2 with a cubic fluorite structure [space group $Fm\bar{3}m$ (225); JCPDS 65-5923] were dominant, and Fe_3O_4 also appeared with a cubic spinel structure [space group $Fd\bar{3}m$ (227); JCPDS 19-0629], as evidenced by the weak diffraction peak from the (311), (511), (440) planes at 35.7°, 59.0°, 63.0°, respectively. The HRTEM image in Figure 1b shows that the particles were regular and uniform with a diameter of 5–10 nm. The lattice fringe spacing of the composite in Figure 1b was about 0.31 nm, which can be assigned to the (111) reflection of CeO_2 with the diffraction peak at 28.6° in Figure 1a. The lattice fringe spacing of the nanoparticles was about 0.25 nm, which can be assigned to the (311) reflection of Fe_3O_4. EDX analysis as seen in Figure S5 (SI) confirmed the coexistence of Fe, Ce, and O in the composite.

As shown in Figure 1c, the nitrogen adsorption–desorption isotherms exhibited typical type IV and hysteresis loops type H3 according to the Brunauer–Deming–Deming–Teller (BDDT) classification, which indicates that Fe_3O_4/CeO_2 composite is typical of a mesoporous structure.[30] The corresponding pore size distribution curve (inset) confirmed that the composite is mainly mesoporous (noting that the mesopore diameter range is defined as 2–50 nm).[31] The BET surface area, pore size, and pore volume of this catalyst were 80.21 m^2 g^{-1}, 3.44 nm, and 0.12 cm^3 g^{-1}, respectively (Table 1).

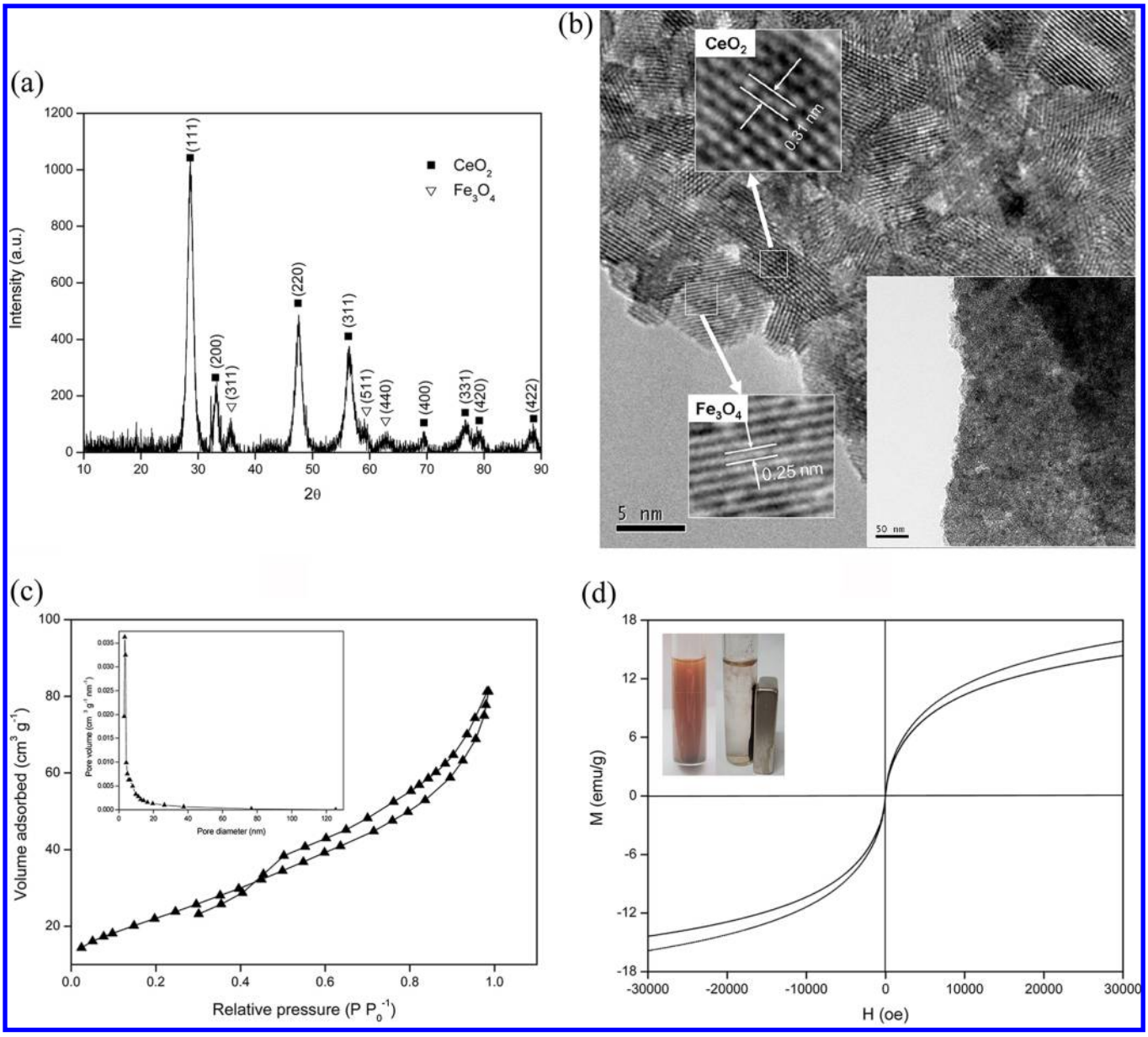

Figure 1. Characterization of Fe_3O_4/CeO_2 composite. (a) XRD pattern. (b) HRTEM images. (c) Nitrogen adsorption−desorption isotherms and pore size distribution curve (the insert pattern) for Fe_3O_4/CeO_2 composite. (d) Magnetization curves of Fe_3O_4/CeO_2 composite before (solid line) and after six reactions (dashed line). The inset pattern is a photograph of the magnetic separation, which shows that the nanoparticles can be separated easily with a magnet.

The room temperature magnetization curves of Fe_3O_4/CeO_2 composite before and after heterogeneous Fenton reactions are shown in Figure 1d. Almost zero coercivity and remanence proves the superparamagnetic properties of the synthesized composite. The saturation magnetization (M_s) of the composite before reaction was found to be 14.4 emu g^{-1}, and after six reactions for 4-CP removal, the M_s value slightly increased to 15.9 emu g^{-1}. These M_s values were a little bit lower than for pure Fe_3O_4 (Table 1), which is mainly attributed to the existence of CeO_2 and the smaller size of composite particles.[32,33] The superparamagnetism shown in Figure 1d (inset) affirmed that the composite could be easily separated and reused from solution by applying an external magnetic field, which is an especially important advantage for nanoparticles.

Catalytic Activity of Fe_3O_4/CeO_2 Composite. Control experiments were conducted to compare the removal efficiencies of 4-CP by various processes at pH 3.0 with initial 4-CP concentration 0.78 mM. The results in Figure 2 show that H_2O_2 only led to a slight removal of 4-CP within 120 min, and a small amount of 4-CP diminished by the CeO_2/H_2O_2 method was primarily ascribed to the surface adsorption of CeO_2 NPs. With 2.0 g/L Fe_3O_4/CeO_2 composite only, about 10% removal was observed mainly due to surface adsorption, which was negligible compared to the fast removal of 4-CP by heterogeneous Fenton reaction. In the presence of H_2O_2, the removal of 4-CP using Fe_3O_4/CeO_2 composite as the heterogeneous Fenton-like catalyst was notably higher than that for pure Fe_3O_4 (Table 1), implying that the catalytic activity was enhanced by the introduction of CeO_2. Furthermore, the degradation of 4-CP by a physical mixture

dx.doi.org/10.1021/es300303f | Environ. Sci. Technol. 2012, 46, 10145−10153

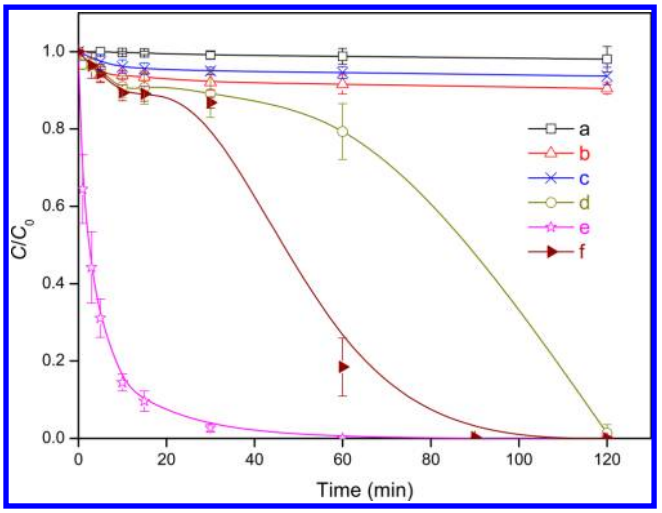

Figure 2. Removal of 4-CP under different conditions: (a) 30 mM H_2O_2; (b) 2.0 g/L Fe_3O_4/CeO_2; (c) 1.0 g/L CeO_2 and 30 mM H_2O_2; (d) 1.0 g/L Fe_3O_4 and 30 mM H_2O_2; (e) 2.0 g/L Fe_3O_4/CeO_2 and 30 mM H_2O_2; (f) 1.0 g/L Fe_3O_4, 1.0 g/L CeO_2, and 30 mM H_2O_2. Other reaction conditions were initial 4-CP concentration 0.78 mM, pH 3.0, and T = 30 °C; C_0 and C are initial 4-CP concentration and its concentration at any time during the reaction, respectively.

of Fe_3O_4 and CeO_2 crystals with H_2O_2 was investigated. Complete removal of 4-CP was achieved after a 90 min reaction, consisting of an induction period and a rapid degradation stage. By comparison, the catalytic activity of Fe_3O_4/CeO_2 composite was higher than that of mixture crystals, suggesting that there might be a synergy effect in the composite, thereby enhancing the relative rates of mass transfer to reactive sites and chemical reaction at reactive sites.

Because the solution pH can remarkably influence the Fenton reaction, the effect of initial pH value on the degradation of 4-CP with Fe_3O_4/CeO_2 catalyst was determined as presented in Figure 3a. About 21% of 4-CP was removed after 120 min of reaction at pH 5.3, and 4-CP degradation increased with the decrease of solution pH. The pseudo-first-order kinetic constants (k) of 4-CP degradation at pH 2.2 and 3.0 were 0.41 and 0.11 min^{-1}, respectively, much higher than that of many reported heterogeneous Fenton-like catalysts.[6,10,11,34]

The pseudo-first-order plots for 4-CP degradation as a function of H_2O_2 dosage (Figure 3b) and Fe_3O_4/CeO_2 composite addition (Figure 3c) were observed. Obviously, the degradation rate constant increased from 0.06 to 0.11 min^{-1} as the H_2O_2 dosage increased from 6 to 30 mM. Hydrogen peroxide is the precursor in the reaction with Fe^{2+} generating

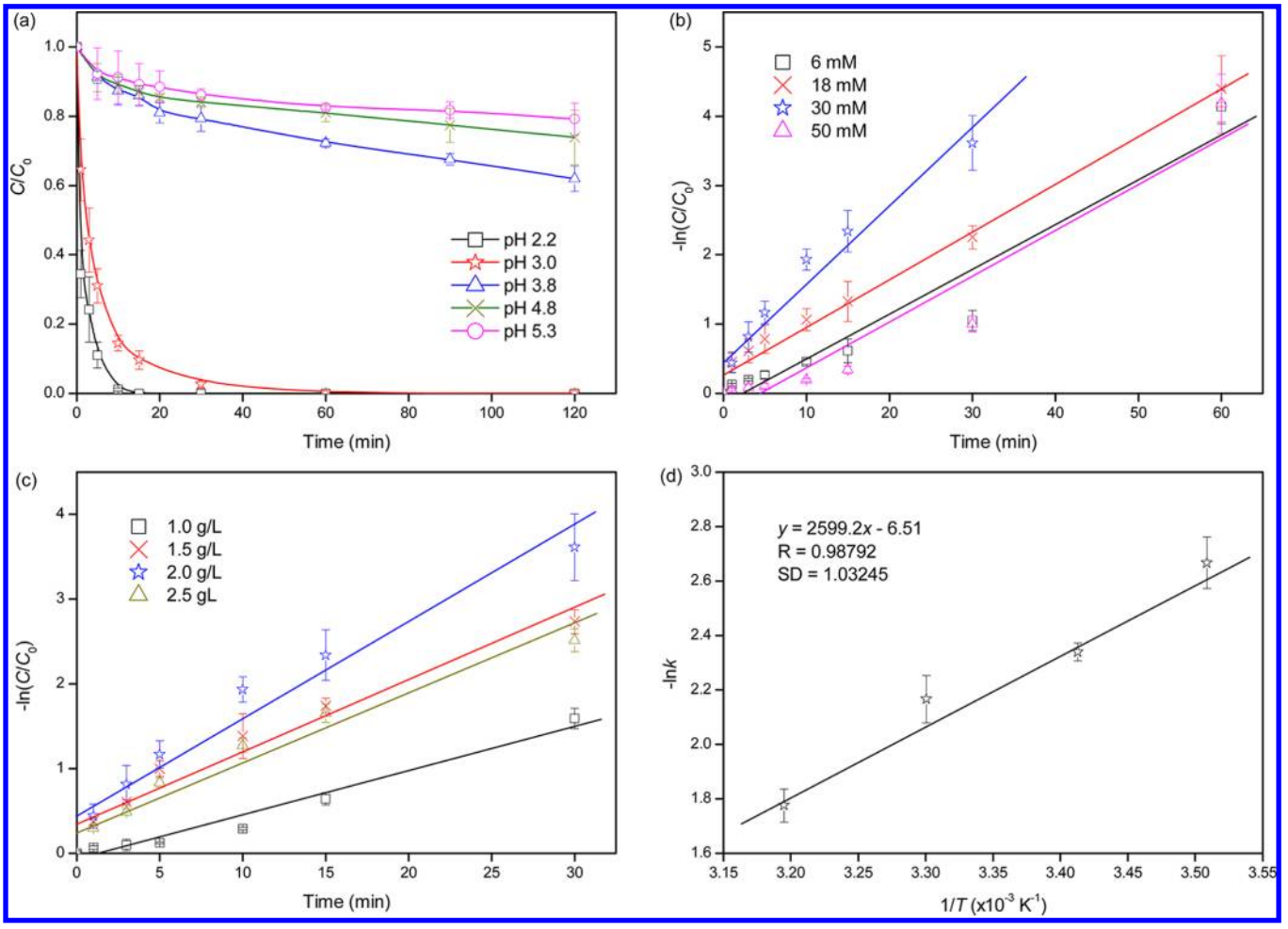

Figure 3. Factorial effects of heterogeneous Fenton reaction on 4-CP degradation: (a) initial pH value, (b) H_2O_2 dosage (where the slope of the plot of $-\ln(C/C_0)$ versus reaction time is the apparent degradation rate constant k), (c) Fe_3O_4/CeO_2 composite addition, and (d) Arrhenius plot based on the effect of temperature. Except for the investigated parameter, other parameters were fixed: pH 3.0, 30 mM H_2O_2, 2.0 g L^{-1} Fe_3O_4/CeO_2, T = 30 °C, and 0.78 mM 4-CP.

hydroxyl radicals (•OH) according to the classical Haber–Weiss mechanism, and it can also react with Fe^{3+} to regenerate Fe^{2+} that can participate in the Fenton reaction. However, with a higher dosage (50 mM), the k value decreased to 0.07 min^{-1}, which is possibly related to the scavenging effect of •OH and the inhibition of iron corrosion by H_2O_2.[1,10] The rate constant increased with an increasing amount of Fe_3O_4/CeO_2 composite from 1.0 to 2.0 g L^{-1} and then slightly decreased. The enhancement of the removal rate may be ascribed to the increasing amount of active sites for the formation of •OH, and the slight decrease of 4-CP removal may be attributed to the agglomeration of nanoparticles and the scavenging of •OH by excess Fe^{2+}.[1,35]

The kinetics of 4-CP degradation was also investigated at different temperatures (12, 20, 30, and 40 °C). The activation energy (E_a) of the reaction on the Fe_3O_4/CeO_2 surface was evaluated by plotting ln k against $1/T$ (Figure 3d) on the basis of the Arrhenius equation and was determined as 21.6 kJ mol^{-1}. This value is higher than the activation energy of the diffusion-controlled reactions, which usually ranges within 10–13 kJ mol^{-1}, implying that the apparent reaction rate for this process is dominated by the rate of intrinsic chemical reactions on the oxide surface rather than the rate of mass transfer.[36,37] The activation energy of Fenton reactions using different heterogeneous catalysts from literature data is between 20.7 and 56.1 kJ mol^{-1},[10,38,39] and the E_a value in our study is at the lower end of the range, indicating that the 4-CP degradation by heterogeneous Fenton reaction requires a relatively low energy and can be easily achieved. Although it is difficult to compare the catalytic activity of various heterogeneous catalysts due to the difference of experimental conditions, all of these results support that Fe_3O_4/CeO_2 composite shows a high catalytic activity in heterogeneous Fenton reaction of 4-CP.

Metal Leaching and H_2O_2 Decomposition. The concentrations of dissolved Fe and Ce in the solution and the utilization efficiency of H_2O_2 were investigated during the Fenton oxidation of 4-CP at pH 3.0 and T = 30 °C with 30 mM H_2O_2, 2.0 g L^{-1} Fe_3O_4/CeO_2, and 0.78 mM 4-CP (adopted as standard reaction conditions). It can be seen from Figure 4 that the concentration of ferrous ion increased and attained a peak value about 3.4 mg L^{-1} at 30 min when almost complete removal of 4-CP occurred (Figure 2), and then Fe^{2+} concentration decreased to about 1.0 mg L^{-1} at 120 min, similar to earlier studies.[40,41] In the ascending period, the oxidation of catalyst by H_2O_2 could release ferrous ions to solution, generating •OH, which corroborated the pseudo-first-order reaction kinetics discussed in the above section. After 4-CP was almost completely removed, the descending period probably resulted from the oxidation of the dissolved ferrous ions to ferric ions by remaining oxidants.[40] Thus, the increase of total dissolved iron could arise from the leaching of ferrous and ferric ions from Fe_3O_4/CeO_2 composite as well as the oxidation of ferrous ions in solution. The loss of iron amounted to 11.8 mg L^{-1}, equivalently about 1.9% of total iron of 2.0 g L^{-1} catalyst used. No detectable amount of dissolved Ce could be measured, indicating that the homogeneous Fenton reaction for 4-CP removal was mainly due to the leaching of Fe in the bulk solution.

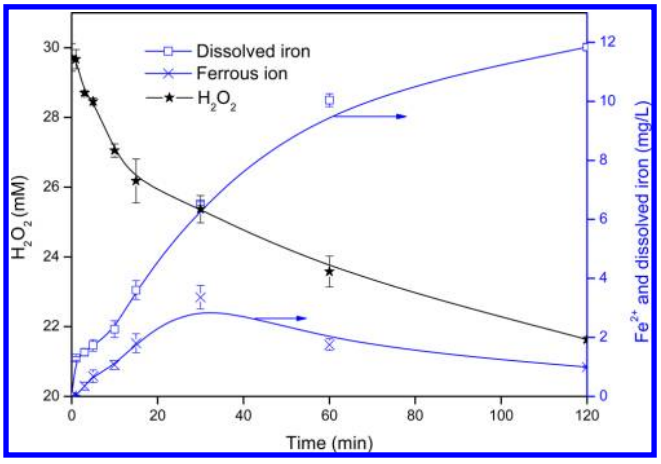

Figure 4. Variation of the concentration of H_2O_2, dissolved iron, and ferrous ion in solution during 4-CP degradation under the standard reaction conditions.

The leaching of Fe was also measured and compared during 4-CP degradation by pure Fe_3O_4 and Fe_3O_4/CeO_2 composite with H_2O_2, as shown in Figure S6 (SI). Slow dissolution of iron was observed in the first 60 min of reaction by the Fe_3O_4/H_2O_2 method, and then the concentrations of ferrous ion and dissolved iron increased to 2.6 and 4.9 mg L^{-1} when 4-CP was completely removed. By comparison, the leaching of iron was much faster during 4-CP degradation by Fe_3O_4/CeO_2 composite than by pure Fe_3O_4. Thus, the component CeO_2 facilitated the dissolution of Fe_3O_4, leading to the enhanced Fenton chemistry, which performed an important function for the removal of 4-CP.

As seen in Figure 4, the concentration of hydrogen peroxide progressively decreased as a function of the time. The stoichiometry utilization efficiency of H_2O_2 was defined as the ratio of the amount of H_2O_2 used for the degradation of pollutants with the total amount of the consumed H_2O_2 in the reaction, as reported by Luo et al.[10] This value was calculated as 79.2% in this study, suggesting a high efficiency of H_2O_2 utilization and a good degradation of 4-CP.

Reusability of Fe_3O_4/CeO_2 MNPs. The recyclability of Fe_3O_4/CeO_2 composite was evaluated by successive batches of 4-CP degradation under the standard reaction conditions. As seen in Figure S7 of the SI, the activity of catalyst decreased gradually during six successive runs after 60 min of reaction, probably due to the leaching of iron from the catalyst surface determined in the former section, which means that the degradation rate of 4-CP was gradually reduced by repeated reuse of the catalyst, thereby prolonging the time for complete removal of 4-CP. After 120 min of reaction, 4-CP was almost completely removed by the reused catalyst, which indicated the possibility of using the catalyst for a longer operation time. Furthermore, the XRD diffraction patterns of the used catalyst were found to be similar to that recorded before reaction (Figure S8, SI). The HRTEM study performed on the particles recovered after six successive catalytic tests showed a possible partial dissolution of the nanoparticles on the catalyst surface (Figure S9, SI). Further work is needed to diminish the leaching of active components from the catalysts and to develop some efficient regeneration procedures.

Possible Degradation Mechanism of 4-CP. The actual reactive species mediated in the process was discriminated by determining the influence of n-butanol and KI as radical scavengers on the degradation of 4-CP, as shown in Figure 5a. Excess n-butanol in solution scavengers all the •OH produced in the system, and iodide ion reacts with surface-bound •OH ($•OH_{ads}$) produced at the surface of Fe_3O_4/CeO_2 particles,

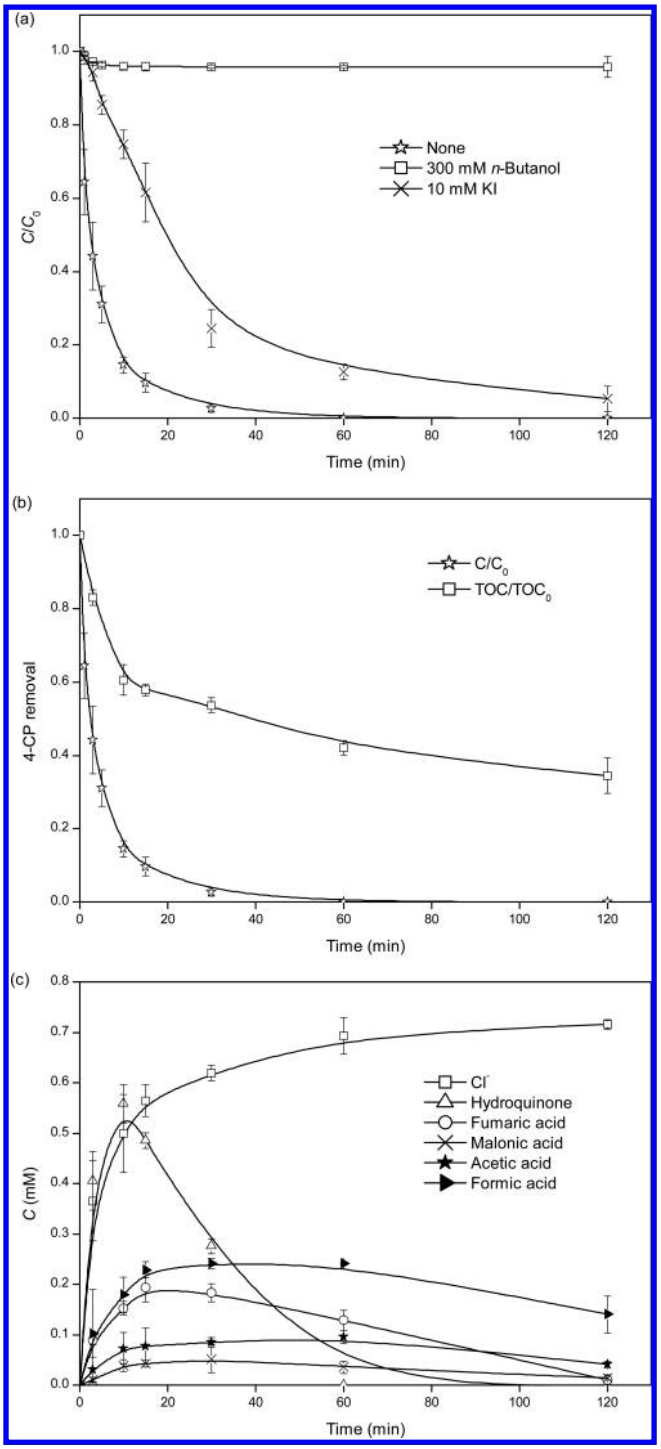

Figure 5. (a) Effect of radical scavengers on the degradation of 4-CP. (b) Temporal change in 4-CP and TOC removal. (c) Evolution of the concentration of chloride ion and intermediates. Reactions were conducted under the standard conditions.

both of which reduce the number of oxidizing species in the system.[1,42,43] The results clearly show that the removal of 4-CP was almost completely inhibited in the presence of 300 mM *n*-butanol, suggesting that 4-CP was oxidized by the attack of •OH both at the surface of catalyst and in the bulk liquid. With addition of excess KI (10 mM), 4-CP degradation decreased from 56%, 69%, 86%, and 90% (in absence of KI) to 6%, 14%, 25%, and 38% at 3, 5, 10, and 15 min, respectively, indicating that $•OH_{ads}$ played a dominant role. After that, about 95% 4-CP removal was achieved at 120 min, mainly attributed to the action of free •OH ($•OH_{free}$) in the bulk solution.

The degree of 4-CP mineralization is shown in Figure 5b, and the results show that the maximum TOC removal obtained after 120 min was 66%, indicating that a residual amount of organic compounds remained in solution. It can be seen from Figure 5c that about 92% of the chlorine was released from the aromatic ring, and hydroquinone as the main intermediate product exhibited a maximum concentration around 15 min, which was then further degraded. As reported by other previous studies, the formation of hydroquinone involves the abstraction of the Cl atom on the para-site of 4-CP by the •OH, leading to a hydroxyphenyl radical that is then coupled with another •OH radical.[44,45] Since catechol was not detected throughout the reaction in our system, the addition of •OH to the ortho-site C atom of 4-CP could be neglected. Hydroquinone was subsequently dehydrogenated to benzoquinone. The ring of benzoquinone was cleaved by the action of •OH to form aliphatic carboxylic acids such as fumaric and malonic acid detected by IC (Figure 5c). Combined with the data presented in Figure 5c, some smaller molecular organic acids such as acetic and formic acid were generated afterward and eventually remained in solution after a reaction time of 120 min associated with the residual TOC value.

Role of Cerium and Ferrum. Surface structure information of Fe_3O_4/CeO_2 composite was analyzed by XPS before and after 4-CP degradation (Figure S10a, SI), and the peaks of binding energy (BE) for Ce 3d, Fe 2p, and O 1s were calibrated with the C 1s BE of 284.6 eV. The atomic ratios of C, O, Fe, and Ce on the surface of the fresh and aged samples are summarized. The surface of Fe_3O_4/CeO_2 contains 5.0% Fe and 9.1% Ce. After 120 min of Fenton oxidation of 4-CP, the atomic ratio of Fe on the surface decreased from 5.0% to 2.9%, while the atomic ratio of Ce remained almost constant. It is consistent with the previous finding of metal leaching, further proving that the homogeneous Fenton reaction in the bulk solution was mainly attributed to the leaching of Fe.

The XPS spectra of Ce 3d for Fe_3O_4/CeO_2 composite before and after reaction are shown in Figure S10b (SI). On the basis of previous works, the Ce 3d spectra are characterized by complex but distinct features arising from the final-state occupation of the Ce 4f level, with the peaks labeled u and v referring to the $3d_{3/2}$ and $3d_{5/2}$ spin−orbit doublets, respectively.[46,47] The doublets denoted u/v, u″/v″, and u‴/v‴ are ascribed to the $3d^{10}4f^0$ initial electronic state of Ce^{4+}, while the u′/v′ doublet is assigned to the $3d^{10}4f^1$ state corresponding to Ce^{3+}.[48,49] For Fe_3O_4/CeO_2 composite before reaction, no distinctive peak ascribed to the Ce^{3+} ion was observed, indicating that the Ce species in Fe_3O_4/CeO_2 catalyst are mostly Ce^{4+}. After 120 min of reaction, as shown in Figure S10b (SI), the small peaks of u′ and v′ evidenced the presence of Ce^{3+}, which could create charge imbalance, the vacancies, and unsaturated chemical bonds on the catalyst surface.[50] The existence of the redox cycle of Ce^{3+} and Ce^{4+} on the surface of the Fe_3O_4/CeO_2 catalyst might play a certain role in heterogeneous Fenton reaction.

The Fe 2p spectra of the fresh and aged samples display the spin−orbit doublet with binding energies of 724.6 eV for Fe 2p1/2 and 711.0 eV for Fe 2p3/2, as shown in Figure S10c (SI). Two components located at 710.7 and 712.2 eV observed for fresh Fe_3O_4/CeO_2 composite are indicative of the presence of Fe(II) and Fe(III), and the peak at 724.6 eV indicates the presence of ferric iron oxides, very close to the BE values

previously reported for magnetite (Fe_3O_4).[39,51] After the reaction with H_2O_2, the area of Fe(II) at BE 710.7 eV was decreased, which could result from the oxidation of Fe(II) to Fe(III) on the surface of Fe_3O_4/CeO_2 associated with a coupled reduction of H_2O_2 to $\bullet OH_{ads}$.

O 1s patterns of XPS were also measured, as shown in Figure S10d (SI). The O 1s peaks at about 529.9−530.3 eV correspond to the lattice oxygen O_I for Fe_3O_4, CeO_2, and Fe_3O_4/CeO_2 catalysts, and another component at about 531.5 eV belongs to the chemisorbed oxygen O_{II}.[50] The chemisorbed oxygen on the Fe_3O_4/CeO_2 catalyst surface is the most active oxygen, which plays an important role in the oxidation reaction. The peak at 530.1 eV observed in the case of rapidly oxidized particles was assigned to oxygen in iron oxides (such as Fe_2O_3),[52] suggesting that oxidation in the Fenton reaction favored the formation of iron oxides, consistent with the observation in the Fe 2p spectrum and the results of dissolved Fe concentration in solution.

On the basis of all the information obtained above, a possible reaction mechanism of the H_2O_2 activation by Fe_3O_4/CeO_2 under acidic condition is proposed in Figure 6. As reported by

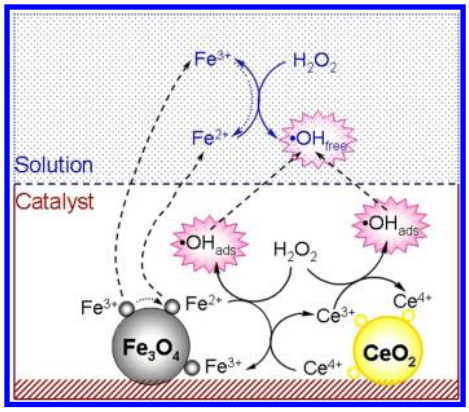

Figure 6. Schematic diagram of the reaction mechanism of the H_2O_2 activation by Fe_3O_4/CeO_2 catalyst under acidic condition.

other researchers,[3,10,11] the initially generated $\equiv Fe^{2+}$ species can react with H_2O_2 to generate surface-bound $\bullet OH_{ads}$ (eq 1), where $\equiv Fe^{2+}$ stands for Fe(II) sites on the catalyst surface. Some more $\equiv Fe^{2+}$ species are produced through the reactions of the formed $\equiv Fe^{3+}$ species with H_2O_2 (eq 2) and $HO_2\bullet$ (eq 3). The standard redox potential of Ce^{4+}/Ce^{3+} is 1.44 V, while that of Fe^{3+}/Fe^{2+} is 0.77 V; hence, the transfer of electrons from $\equiv Fe^{2+}$ to $\equiv Ce^{4+}$ (eq 4) is thermodynamically favored. Cerium is capable of redox cycling in the presence of H_2O_2 and produces $\bullet OH_{ads}$ (eqs 5−7), behaving similarly to iron in a Fenton-like reaction, which is also proposed by Heckert et al.[15] Dissolved iron (Fe^{2+} and Fe^{3+}) resulted from dissolution of iron oxides disperse into bulk solution and initiate the decomposition of H_2O_2 through a chain reaction (eqs 8−10), producing $\bullet OH_{free}$. A minimal amount of $\bullet OH_{ads}$ can diffuse from the surface of the catalyst into the bulk solution. Furthermore, the competitive reactions that can negatively affect the oxidation process occur, as seen in eqs 11−16. Finally, 4-CP is broken down mainly by hydroxyl radicals including $\bullet OH_{ads}$ on the surface of catalyst and $\bullet OH_{free}$ in the bulk solution.

$$\equiv Fe^{2+} + H_2O_2 + H^+ \rightarrow \equiv Fe^{3+} + \bullet OH_{ads} + H_2O \quad (1)$$

$$\equiv Fe^{3+} + H_2O_2 \rightarrow \equiv Fe^{2+} + HO_2\bullet + H^+ \quad (2)$$

$$\equiv Fe^{3+} + HO_2\bullet \rightarrow \equiv Fe^{2+} + O_2 + H^+ \quad (3)$$

$$\equiv Ce^{4+} + \equiv Fe^{2+} \leftrightarrow \equiv Ce^{3+} + \equiv Fe^{3+} \quad (4)$$

$$\equiv Ce^{3+} + H_2O_2 + H^+ \rightarrow \equiv Ce^{4+} + \bullet OH_{ads} + H_2O \quad (5)$$

$$\bullet OH_{ads} + H_2O_2 \rightarrow HO_2^- + H_2O \quad (6)$$

$$\equiv Ce^{4+} + HO_2^- \rightarrow \equiv Ce^{3+}H^+ + O_2 \quad (7)$$

$$Fe^{2+} + H_2O_2 + H^+ \rightarrow Fe^{3+} + \bullet OH_{free} + H_2O \quad (8)$$

$$Fe^{3+} + H_2O_2 \rightarrow Fe^{2+} + HO_2\bullet + H^+ \quad (9)$$

$$Fe^{3+} + HO_2\bullet \rightarrow Fe^{2+} + O_2 + H^+ \quad (10)$$

$$\bullet OH + Fe^{2+} \rightarrow OH^- + Fe^{3+} \quad (11)$$

$$\bullet OH + H_2O_2 \rightarrow H_2O + HO_2\bullet \quad (12)$$

$$Fe^{2+} + HO_2\bullet \rightarrow Fe^{3+} + HOO^- \quad (13)$$

$$HO_2\bullet + HO_2\bullet \rightarrow H_2O_2 + O_2 \quad (14)$$

$$\bullet OH + HO_2\bullet(O_2\bullet^-) \rightarrow O_2 + H_2O(+OH^-) \quad (15)$$

$$\bullet OH + \bullet OH \rightarrow H_2O_2 \quad (16)$$

$$\bullet OH + 4\text{-CP} \rightarrow \text{degraded products} \quad (17)$$

■ ASSOCIATED CONTENT

Supporting Information

Additional information as noted in the text. This material is available free of charge via the Internet at http://pubs.acs.org.

■ AUTHOR INFORMATION

Corresponding Author

*Phone: 86-10-62784843; fax: 86-10-62771150; e-mail: wangjl@tsinghua.edu.cn.

Notes

The authors declare no competing financial interest.

■ ACKNOWLEDGMENTS

The authors are grateful for the financial support provided by the National Natural Science Foundation of China (Grant nos. 50978145; 51078210).

■ REFERENCES

(1) Xu, L. J.; Wang, J. L. A heterogeneous Fenton-like system with nanoparticulate zero-valent iron for oxidation of 4-chloro-3-methyl phenol. *J. Hazard. Mater.* **2011**, *186* (1), 256−264.

(2) Deng, J. H.; Jiang, J. Y.; Zhang, Y. Y.; Lin, X. P.; Du, C. M.; Xiong, Y. $FeVO_4$ as a highly active heterogeneous Fenton-like catalyst towards the degradation of Orange II. *Appl. Catal. B: Environ.* **2008**, *84* (3−4), 468−473.

(3) Costa, R. C. C.; Moura, F. C. C.; Ardisson, J. D.; Fabris, J. D.; Lago, R. M. Highly active heterogeneous Fenton-like systems based on Fe^0/Fe_3O_4 composites prepared by controlled reduction of iron oxides. *Appl. Catal. B: Environ.* **2008**, *83* (1−2), 131−139.

(4) Oliveira, L. C. A.; Gonçalves, M.; Guerreiro, M. C.; Ramalho, T. C.; Fabris, J. D.; Pereira, M. C.; Sapag, K. A new catalyst material based on niobia/iron oxide composite on the oxidation of organic

contaminants in water via heterogeneous Fenton mechanisms. *Appl. Catal., A* **2007**, *316* (1), 117−124.
(5) Navalon, S.; Alvaro, M.; Garcia, H. Heterogeneous Fenton catalysts based on clays, silicas and zeolites. *Appl. Catal. B: Environ.* **2010**, *99* (1−2), 1−26.
(6) Zhang, G. K.; Gao, Y. Y.; Zhang, Y. L.; Guo, Y. D. Fe_2O_3-pillared rectorite as an efficient and stable Fenton-like heterogeneous catalyst for photodegradation of organic contaminants. *Environ. Sci. Technol.* **2010**, *44* (16), 6384−6389.
(7) Herney-Ramirez, J.; Vicente, M. A.; Madeira, L. M. Heterogeneous photo-Fenton oxidation with pillared clay-based catalysts for wastewater treatment: A review. *Appl. Catal. B: Environ.* **2010**, *98* (1−2), 10−26.
(8) Zhong, X.; Royer, S.; Zhang, H.; Huang, Q. Q.; Xiang, L. J.; Valange, S.; Barrault, J. Mesoporous silica iron-doped as stable and efficient heterogeneous catalyst for the degradation of CI Acid Orange 7 using sono-photo-Fenton process. *Sep. Purif. Technol.* **2011**, *80* (1), 163−171.
(9) Zhang, J. B.; Zhuang, J.; Gao, L. Z.; Zhang, Y.; Gu, N.; Feng, J.; Yang, D. L.; Zhu, J. D.; Yan, X. Y. Decomposing phenol by the hidden talent of ferromagnetic nanoparticles. *Chemosphere* **2008**, *73* (9), 1524−1528.
(10) Luo, W.; Zhu, L. H.; Wang, N.; Tang, H. Q.; Cao, M. J.; She, Y. B. Efficient removal of organic pollutants with magnetic nanoscaled $BiFeO_3$ as a reusable heterogeneous Fenton-like catalyst. *Environ. Sci. Technol.* **2010**, *44* (5), 1786−1791.
(11) Hu, X. B.; Liu, B. Z.; Deng, Y. H.; Chen, H. Z.; Luo, S.; Sun, C.; Yang, P.; Yang, S. G. Adsorption and heterogeneous Fenton degradation of 17α-methyltestosterone on nano Fe_3O_4/MWCNTs in aqueous solution. *Appl. Catal. B: Environ.* **2011**, *107* (3−4), 274−283.
(12) Gao, L. Z.; Zhuang, J.; Nie, L.; Zhang, J. B.; Zhang, Y.; Gu, N. W., T. H.; Feng, J.; Yang, D. L.; Perrett, S.; Yan, X. Y. Intrinsic peroxidase-like activity of ferromagnetic nanoparticles. *Nat. Nanotechnol.* **2007**, *9* (2), 577−583.
(13) Campbell, C. T.; Peden, C. H. F. Oxygen vacancies and catalysis on ceria surfaces. *Science* **2005**, *309* (5735), 713−714.
(14) Esch, F.; Fabris, S.; Zhou, L.; Montini, T.; Africh, C.; Fornasiero, P.; Comelli, G.; Rosei, R. Electron localization determines defect formation on ceria substrates. *Science* **2005**, *309* (5735), 752−755.
(15) Heckert, E. G.; Seal, S.; Self, W. T. Fenton-like reaction catalyzed by the rare earth inner transition metal cerium. *Environ. Sci. Technol.* **2008**, *42* (13), 5014−5019.
(16) Ozawa, M.; Loong, C. K. In situ X-ray and neutron powder diffraction studies of redox behavior in CeO_2-containing oxide catalysts. *Catal. Today* **1999**, *50* (2), 329−342.
(17) Song, S.; Xu, L. J.; He, Z. Q.; Chen, J. M.; Xiao, X. Z.; Yan, B. Mechanism of the photocatalytic degradation of C.I. Reactive Black 5 at pH 12.0 using $SrTiO_3/CeO_2$ as the catalyst. *Environ. Sci. Technol.* **2007**, *41*, 5846−5853.
(18) Song, S.; Xu, L. J.; He, Z. Q.; Ying, H. P.; Chen, J. M.; Xiao, X. Z.; Yan, B. Photocatalytic degradation of C.I. Direct Red 23 in aqueous solutions under UV irradiation using $SrTiO_3/CeO_2$ composite as the catalyst. *J. Hazard. Mater.* **2008**, *152* (3), 1301−1308.
(19) Martins, R. C.; Amaral-Silva, N.; Quinta-Ferreira, R. M. Ceria based solid catalysts for Fenton's depuration of phenolic wastewaters, biodegradability enhancement and toxicity removal. *Appl. Catal. B: Environ.* **2010**, *99* (1−2), 135−144.
(20) Rossi, A. F.; Amaral-Silva, N.; Martins, R. C.; Quinta-Ferreira, R. M. Heterogeneous Fenton using ceria based catalysts: Effects of the calcination temperature in the process efficiency. *Appl. Catal. B: Environ.* **2012**, *111*, 254−263.
(21) Zhang, Y.; Dou, X. M.; Liu, J.; Yang, M.; Zhang, L. P.; Kamagata, Y. Decolorization of reactive Brilliant Red X-3B by heterogeneous photo-Fenton reaction using an Fe−Ce bimetal catalyst. *Catal. Today* **2007**, *126* (3−4), 387−393.
(22) Jiang, X. Y.; Lu, G. L.; Zhou, R. X.; Mao, J. X.; Chen, Y.; Zheng, X. M. Studies of pore structure, temperature-programmed reduction performance, and micro-structure of CuO/CeO_2 catalysts. *Appl. Surf. Sci.* **2001**, *173* (3−4), 208−220.
(23) Yee, A.; Morrison, S. J.; Idriss, H. The reactions of ethanol over M/CeO_2 catalysts - Evidence of carbon−carbon bond dissociation at low temperatures over Rh/CeO_2. *Catal. Today* **2000**, *63* (2−4), 327−335.
(24) Kim, D. K.; Mikhaylova, M.; Zhang, Y.; Muhammed, M. Protective coating of superparamagnetic iron oxide nanoparticles. *Chem. Mater.* **2003**, *15* (8), 1617−1627.
(25) Tamura, H.; Goto, K.; Yotsuyan., T; Nagayama, M. Spectrophotometric determination of iron(II) with 1,10-Phenanthroline in presence of large amounts of iron(III). *Talanta* **1974**, *21* (4), 314−318.
(26) Lee, C.; Keenan, C. R.; Sedlak, D. L. Polyoxometalate-enhanced oxidation of organic compounds by nanoparticulate zero-valent iron and ferrous ion in the presence of oxygen. *Environ. Sci. Technol.* **2008**, *42* (13), 4921−4926.
(27) Pham, A. L. T.; Lee, C.; Doyle, F. M.; Sedlak, D. L. A silica-supported iron oxide catalyst capable of activating hydrogen peroxide at neutral pH values. *Environ. Sci. Technol.* **2009**, *43* (23), 8930−8935.
(28) Kavitha, V.; Palanivelu, K. The role of ferrous ion in Fenton and photo-Fenton processes for the degradation of phenol. *Chemosphere* **2004**, *55* (9), 1235−1243.
(29) Xu, L. J.; Wang, J. L. Fenton-like degradation of 2,4-dichlorophenol using Fe_3O_4 magnetic nanoparticles. *Appl. Catal. B: Environ.* **2012**, *123−124*, 117−126.
(30) Kruk, M.; Jaroniec, M. Gas adsorption characterization of ordered organic−inorganic nanocomposite materials. *Chem. Mater.* **2001**, *13* (10), 3169−3183.
(31) Duarte, F.; Maldonado-Hódar, F. J.; Pérez-Cadenas, A. F.; Madeira, L. M. Fenton-like degradation of azo-dye Orange II catalyzed by transition metals on carbon aerogels. *Appl. Catal. B: Environ.* **2009**, *85* (3−4), 139−147.
(32) Ge, J. P.; Hu, Y. X.; Biasini, M.; Beyermann, W. P.; Yin, Y. D. Superparamagnetic magnetite colloidal nanocrystal clusters. *Angew. Chem., Int. Ed.* **2007**, *46* (23), 4342−4345.
(33) Thi, D. N.; Ngoc, H. P.; Manh, H. D.; Kim, T. N. Magnetic Fe_2MO_4 (M:Fe, Mn) activated carbons: Fabrication, characterization and heterogeneous Fenton oxidation of Methyl Orange. *J. Hazard. Mater.* **2011**, *185* (2−3), 653−661.
(34) Panda, N.; Sahoo, H.; Mohapatra, S. Decolourization of Methyl Orange using Fenton-like mesoporous Fe_2O_3−SiO_2 composite. *J. Hazard. Mater.* **2011**, *185* (1), 359−365.
(35) Liao, Q.; Sun, J.; Gao, L. Degradation of phenol by heterogeneous Fenton reaction using multi-walled carbon nanotube supported Fe_2O_3 catalysts. *Colloids Surf. Physicochem. Eng. Aspects* **2009**, *345* (1−3), 95−100.
(36) Lin, S. S.; Gurol, M. D. Catalytic decomposition of hydrogen peroxide on iron oxide: Kinetics, mechanism, and implications. *Environ. Sci. Technol.* **1998**, *32* (10), 1417−1423.
(37) Xue, X. F.; Hanna, K.; Abdelmoula, M.; Deng, N. S. Adsorption and oxidation of PCP on the surface of magnetite: Kinetic experiments and spectroscopic investigations. *Appl. Catal. B: Environ.* **2009**, *89* (3−4), 432−440.
(38) Dükkanci, M.; Gündüz, G.; Yilmaz, S.; Prihod'ko, R. V. Heterogeneous Fenton-like degradation of Rhodamine 6G in water using CuFeZSM-5 zeolite catalyst prepared by hydrothermal synthesis. *J. Hazard. Mater.* **2010**, *181* (1−3), 343−350.
(39) Ramirez, J. H.; Maldonado-Hódar, F. J.; Pérez-Cadenas, A. F.; Moreno-Castilla, C.; Costa, C. A.; Madeira, L. M. Azo-dye Orange II degradation by heterogeneous Fenton-like reaction using carbon−Fe catalysts. *Appl. Catal. B: Environ.* **2007**, *75* (3−4), 312−323.
(40) Luo, M. L.; Bowden, D.; Brimblecombe, P. Catalytic property of Fe-Al pillared clay for Fenton oxidation of phenol by H_2O_2. *Appl. Catal. B: Environ.* **2009**, *85* (3−4), 201−206.
(41) Feng, J. Y.; Hu, X. J.; Yue, P. L. Discoloration and mineralization of Orange II using different heterogeneous catalysts containing Fe: A comparative study. *Environ. Sci. Technol.* **2004**, *38* (21), 5773−5778.
(42) He, Z. Q.; Song, S.; Ying, H. P.; Xu, L. J.; Chen, J. M. *p*-Aminophenol degradation by ozonation combined with sonolysis:

Operating conditions influence and mechanism. *Ultrason. Sonochem.* **2007**, *14* (5), 568−574.
(43) Martin, S. T.; Lee, A. T.; Hoffmann, M. R. Chemical mechanism of inorganic oxidants in the TiO_2/UV process: Increased rates of degradation of chlorinated hydrocarbons. *Environ. Sci. Technol.* **1995**, *29* (10), 2567−2573.
(44) Wang, H.; Wang, J. L. Electrochemical degradation of 4-chlorophenol using a novel Pd/C gas-diffusion electrode. *Appl. Catal. B: Environ.* **2007**, *77* (1−2), 58−65.
(45) Yang, J.; Dai, J.; Chen, C. C.; Zhao, J. C. Effects of hydroxyl radicals and oxygen species on the 4-chlorophenol degradation by photoelectrocatalytic reactions with TiO_2-film electrodes. *J. Photochem. Photobiol. A: Chem.* **2009**, *208* (1), 66−77.
(46) Burroughs, P.; Hamnett, A.; Orchard, A. F.; Thornton, G. Satellite structure in X-ray photoelectron-spectra of some binary and mixed oxides of lanthanum and cerium. *J. Chem. Soc. Dalton* **1976**, *17*, 1686−1698.
(47) Reddy, B. M.; Khan, A.; Yamada, Y.; Kobayashi, T.; Loridant, S.; Volta, J. C. Structural characterization of CeO_2−TiO_2 and V_2O_5/CeO_2−TiO_2 catalysts by Raman and XPS techniques. *J. Phys. Chem. B* **2003**, *107* (22), 5162−5167.
(48) Li, H. L.; Wu, C. Y.; Li, Y.; Zhang, J. Y. CeO_2−TiO_2 catalysts for catalytic oxidation of elemental mercury in low-rank coal combustion flue gas. *Environ. Sci. Technol.* **2011**, *45* (17), 7394−7400.
(49) Song, S.; Tu, J. J.; Xu, L. J.; Xu, X.; He, Z. Q.; Qiu, J. P.; Ni, J. G.; Chen, J. M. Preparation of a titanium dioxide photocatalyst codoped with cerium and iodine and its performance in the degradation of oxalic acid. *Chemosphere* **2008**, *73* (9), 1401−1406.
(50) Yang, S. X.; Zhu, W. P.; Jiang, Z. P.; Chen, Z. X.; Wang, J. B. The surface properties and the activities in catalytic wet air oxidation over CeO_2−TiO_2 catalysts. *Appl. Surf. Sci.* **2006**, *252* (24), 8499−8505.
(51) Zhu, Y.; Tian, L.; Jiang, Z.; Pei, Y.; Xie, S. H.; Qiao, M. H.; Fan, K. N. Heteroepitaxial growth of gold on flowerlike magnetite: An efficacious and magnetically recyclable catalyst for chemoselective hydrogenation of crotonaldehyde to crotyl alcohol. *J. Catal.* **2011**, *281* (1), 106−118.
(52) Li, P. N.; Zhang, L. Z.; Wang, W. W.; Su, J. L.; Feng, L. L. Rapid catalytic microwave method to damage *Microcystis aeruginosa* with $FeCl_3$-loaded active carbon. *Environ. Sci. Technol.* **2011**, *45* (10), 4521−4526.